Nanoscale

Accepted Manuscript

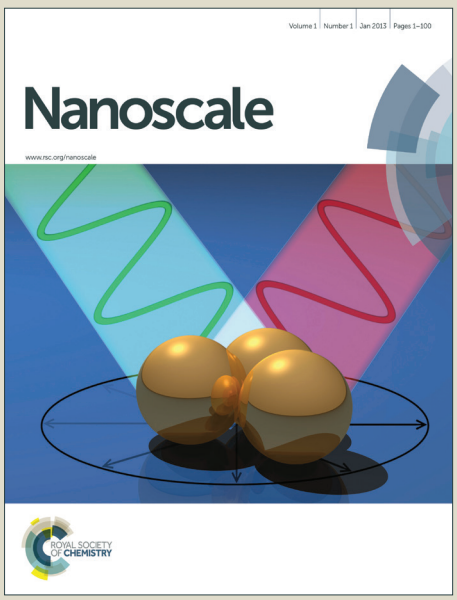

ROYAL SOCIETY OF CHEMISTRY

www.rsc.org/nanoscale

Cite this: DOI: 10.1039/c0xx00000x

www.rsc.org/xxxxxx

ARTICLE TYPE

Graphene oxide and shape-controlled silver nanoparticle hybrid for ultrasensitive single-particle surface-enhanced Raman scattering (SERS) sensing †

Wei Fan,[a,b] Yih Hong Lee,[a] Srikanth Pedireddy,[a] Qi Zhang,[a] Tianxi Liu*[b] and Xing Yi Ling*[a]

Received (in XXX, XXX) Xth XXXXXXXXX 200X, Accepted Xth XXXXXXXXX 200X
DOI: 10.1039/b000000x

Graphene oxide (GO) is an emerging material for surface-enhanced Raman scattering (SERS) due to its strong chemical enhancement. Studying the SERS performance of plasmonic nanoparticle/GO hybrid materials at the single particle level is crucial for direct probing of the chemical effect of GO on plasmonic nanoparticles. In this work, we integrate GO and shaped-controlled Ag nanoparticles to create hybrid nanomaterials, and the chemical enhancement arising from GO is investigated using single–particle SERS measurements. Ag nanoparticle@GO hybrid nanostructures are prepared by assembling Ag nanoparticles, including spheres, cubes and octahedral with GO sheets. The SERS behaviors of the hybrid nanostructures are characterized, and 2-3 times enhanced SERS intensities are detected from the Ag nanoparticle@GO hybrid nanostructures as compared to pure Ag nanoparticles. Furthermore, we probe the mechanism of SERS enhancement in the hybrid nanostructures by changing the surface coverage of GO on Ag octahedra, by using reduced GO in place of GO as well as by using probe molecules of different electronegativity. This hybrid system as is an excellent candidate for single-particle SERS sensor. Sub-nanomolar level of aromatic molecules is detected using single Ag/GO hybrid nanomaterial. This as-prepared GO and shaped-controlled Ag nanoparticle hybrid is capable of serving as high performance SERS platform, providing new opportunities for efficient chemical and biological sensing applications.

1. Introduction

Surface-enhanced Raman scattering (SERS) has proven to be an ultra-sensitive and powerful analytical technique for molecular sensing and detection, with the ability to detect single molecules already demonstrated in the literature.[1-7] The impressive sensitivity of SERS over Raman spectroscopy stems from two enhancement mechanisms, namely electromagnetic and chemical enhancements. Electromagnetic enhancement is most commonly associated with the localized surface plasmon resonances (LSPRs) of noble metal nanoparticles, such as those of Au and Ag. LSPRs are capable of concentrating incident light into sub-wavelength volumes around the nanoparticles, thereby generating intense localized electromagnetic fields.[8-11] It has been shown that localized electromagnetic fields are most intense near regions with large radius of curvatures (sharp tips/edges) or having high asperities. While electromagnetic enhancement involving metal nanoparticles are well studied, chemical enhancement in related systems remains a debatable topic to date.[12-14]

On the other hand, graphene and related materials, such as graphene oxide (GO) and reduced graphene oxide (RGO), have been shown to be an emerging material of choice as SERS substrates due to strong chemical enhancement.[15-21] This class of materials is atomically flat, and enables efficient charge transfer due to the short separation distance between graphene and probe molecules. Chemical enhancement is thought to originate from the $\pi - \pi$ interactions and charge transfer from oxygen-rich functional groups on graphene and related materials.[18] Importantly, it has been shown that the most efficient chemical enhancement occurs for imperfect graphene, i.e. graphene possessing charge transfer groups. The oxidation and p-doping of graphene has been shown to bring about a chemical enhancement of 10^4-fold on aromatic dye molecules, an order higher than pristine graphene.[20] Mildly reduced GO has also been shown to lead to enhancement factors around 10^3.[21]

Given the superior SERS capabilities of both metallic nanoparticles and graphene based materials, there are increasing studies focused on investigating the SERS efficiencies of composites of metallic nanoparticles and graphene. SERS signals arising from graphene/metal hybrid structures are also shown to have higher SERS signals when compared to the individual components.[22-28] For instance, SERS signals of probe molecules such as rhodamine 6G and methylene blue are shown to be further enhanced several-fold when compared against those of pure metallic nanoparticles, with detection limits reaching nanomolar (nM) levels.[28] Furthermore, such composite materials have also shown good sensitivity towards sensing hydrogen

peroxide,[29,30] folic acid,[31] uranyl ions,[32] multiplexed DNA detection[33] and differentiation of neural stem cells.[34]

However, among the extensive reports on the SERS capabilities of ensembled graphene-based metal nanoparticle hybrid materials, most of the Ag nanoparticles reported previously are spherical ones. Ag architectures with unique shape and morphology, such as cubes or octahedra have not been reported yet. Moreover, SERS signals are usually obtained from clusters of Ag nanoparticles or Ag nanoparticle aggregates. In addition, there is a lack of studies on the SERS capabilities at the single particle level. Single-particle SERS measurements are crucial for direct probing of the chemical enhancement effect without the interference from electromagnetic field enhancement arising from the plasmonic coupling among ensembled neighboring nanoparticles.

Herein, we investigate the single-particle SERS efficiencies of Ag nanoparticles/GO and their SERS sensing capabilities. We aim to directly investigate the chemical enhancement arising from GO, and obtain an optimal Ag/GO configuration that gives the highest SERS sensitivity. Morphologically-controlled Ag nanoparticles, including spheres, cubes and octahedra, are assembled with GO sheets to form Ag nanoparticles@GO hybrid nanostructures. The SERS behaviors of the hybrid nanostructures are characterized using single-particle SERS measurements, and enhanced SERS intensities are detected from the Ag nanoparticles@GO hybrid nanostructures as compared to pure Ag nanoparticles. A strong particle morphology-dependent trend in the SERS signals measured is observed. Furthermore, we probe the mechanism of SERS enhancement in the hybrid nanostructures by using GO with different degrees of reduction and also by using various probe molecules. Our single-particle Ag/GO hybrid is used as a SERS sensor for aromatic molecules, which is capable of detecting nanomolar levels of aromatic molecules.

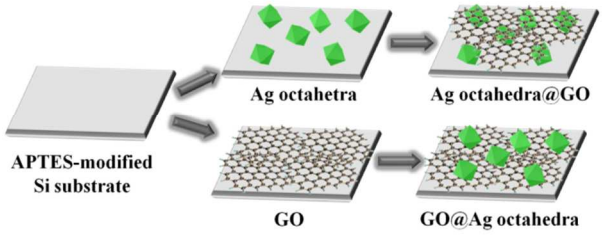

Fig. 1 Schematic illustration of the fabrication of Ag octahedra@GO and GO@Ag octahedra hybrids on APTES-modified silicon substrates.

2. Experimental Section

2.1 Materials

Natural graphite powder (325 mesh) was purchased from Alfa-Aesar. Silver nitrate ($AgNO_3$, 99%), poly(vinyl pyrrolidone) (PVP, $M_w \approx 55\,000$ g/mol), 1,5-pentanediol, 4-methylbenzenethiol (4-MBT, 98%), 4-mercaptobenzoicacid (4-MBA, 90%), 4-aminothiophenol (4-ATP, 97%) and 3-aminopropyltriethoxysilane (APTES) were all obtained from Sigma-Aldrich. Rhodamine 6G (R6G) and crystal violet (CV) from Sigma-Aldrich were used as Raman probes. All chemicals were used as received without further treatment. Deionized water (resistance > 18.0 MΩ cm^{-1}) was used throughout all the experiments.

2.2 Synthesis of GO and Ag nanoparticles

Graphite oxide was synthesized from natural graphite powder by a modified Hummers method.[35] In brief, 1.5 g graphite powder was added into a mixture of 10 mL 98% H_2SO_4, 1.25 g $K_2S_2O_8$, and 1.25 g P_2O_5, and the solution was maintained at 80 °C for 4.5 h. The resulting pre-oxidized product was cleaned with water and dried in a vacuum oven at 50 °C. After it was mixed with 60 mL 98% H_2SO_4 and slowly added 7.5 g $KMnO_4$ at a temperature below 20 °C, then 125 mL H_2O was added. After 2 h, additional 200 mL H_2O and 10 mL 30% H_2O_2 were slowly added into the solution to completely react with the excess $KMnO_4$. After 10 min, a bright yellow solution was obtained. The resulting mixture was washed with diluted HCl aqueous (1/10 v/v) solution and H_2O. The graphite oxide was obtained after drying in a vacuum oven at 30 °C. Exfoliation was carried out by sonicating 0.5 mg/mL graphite oxide dispersion under ambient condition for 30 min. The resulted homogeneous dispersion (GO) colored yellow-brown was diluted to 0.05 mg/mL for further use. In a typical procedure for chemical conversion of GO to RGO, the resulting homogeneous dispersion was mixed with hydrazine solution and ammonia solution. The weight ratio of hydrazine to GO was about 7:10. The solution was then heated to 95 °C for 1 h and 6 h to get $RGO_{7/3}$ and $RGO_{9/1}$, respectively.

Silver nanocubes and octahedra were synthesized according to a method as reported previously.[36] In brief, Silver nitrate (0.20 g) and copper(II) chloride (0.08 mg) were prepared separately in 10 mL 1,5-pentanediol. The chemicals were sonicated and vortexed repeatedly to dissolve them. 35 μL $CuCl_2$ solution was then added to the $AgNO_3$ solution. In a separate vial, PVP (0.20 g) was dissolved in 1,5-pentanediol (10 mL). All solutions were dissolved using ultrasonic baths. Using a temperature-controlled silicone oil bath, 1,5-pentanediol (20 mL) was heated for 10 min in the 190 °C oil bath. The two precursor solutions were then injected into the hot reaction flask at the following rates: 500 μL of the silver nitrate solution every minute and 250 μL of the PVP solution every 30 s. For nanocubes, this addition was stopped once the solution turned opaque (~20 min). For octahedra, the mixture was continuously heated at 190 °C for 10 min and then the injections of silver nitrate and PVP solutions were resumed and continued for a longer period of time (60-75 min). Silver nanospheres was prepared by an aqueous reduction of silver nitrate with trisodium citrate using a method of Lee and Meisel,[37] and silver film (~100 nm in thickness) were deposited at a rate of about 1 Å/s by thermal evaporation.

2.3 Preparation of APTES-modified silicon substrates

Silicon wafer with evaporated chromium pattern was used as an index finder for SEM correlation. The substrate was cleaned by sequential ultrasonication in acetone, ethanol, deionized water for 15 min in each and then treated with oxygen plasma at 80 W for 5 min to derive a hydroxyl surface. After thorough rinsing with ethanol, the cleaned glass substrate was dried under a stream of nitrogen. Subsequently, the cleaned silicon substrate was immersed in a 10% solution of APTES in ethanol for 16 h to functionalize the Si surface with amino-functional groups. The

substrate was then rinsed profusely with ethanol to remove unbound molecules from the surface and dried under a stream of nitrogen.

2.4 Fabrication of GO and Ag nanoparticles hybrid

For Raman spectroscopy, probe molecules coated Ag nanoparticles were prepared by exchanging the PVP with 4-MBT in a 10 mM ethanolic solution, which was stirred for 12 h at room temperature under a stream of nitrogen to minimize oxidation. Similarly, 4-ATP and 4-MBA coated Ag octahedra were prepared by the same procedure. For fabrication of GO and Ag octahedra hybrid, a dilute solution of Ag octahedra suspending in ethanol were drop-casted onto the APTES-modified Si substrates, washed with ethanol, and dried under a stream of nitrogen. Subsequently, the substrate was immersed in GO suspension (0.05 mg/mL) for 2 h, washed with water, and dried under a stream of nitrogen. The as-prepared GO on top of Ag octahedra hybrid was denoted as Ag octahedra@GO, and GO@Ag octahedra hybrid with GO underneath Ag octahedra were also prepared in a similar process but in inverse assemble sequence. In addition, other shapes of Ag nanoparticles and GO hybrids were also prepared similarly for comparison.

2.5 Characterization

Field emission scanning electron microscopy (FESEM) characterization was conducted with a JSM-7600F SEM at an accelerating voltage of 5 kV. Transmission electron microscopy (TEM) observation was performed with a JEOL 2100 TEM under an accelerating voltage of 200 kV. Tapping mode atomic force microscopy (AFM) images were taken using a scanning probe microscope Nanoscope IV (Digital Instruments). The surface charge of the oppositely charged GO sheets synthesized was measured using a ζ–potential analyzer (Malvern, Zetasizer Nano ZS). X-ray photoelectron spectroscopy (XPS) spectra were measured using a Phoibos 100 spectrometer with a monochromatic Mg X-ray radiation source. All XPS spectra were fit using XPS Peak 4.1.

2.6 Surface-enhanced Raman scattering

Raman spectroscopy was obtained by the Ramantouch microspectrometer (Nanophoton Inc, Osaka, Japan). All mapping experiments were carried out with a 100 × objective lens (NA = 0.9) and were taken using 10 s acquisition time between 127 and 2672 cm^{-1}. To obtain single-particle spectra, laser powers of 0.17 mW were used for 532 nm excitations. Automated mapping software was used to control the movement of the stage in 0.5 μm steps during the mapping experiments. Use of the confocal pinhole ensured that the illumination area for each of the wavelengths was comparable. After the Raman mapping was complete, the chromium pads aided in pattern matching with SEM images to ensure that only single particles were used for quantification.

3. Results and discussion

GO sheets and Ag nanocrystals are separately prepared for this study. GO sheets are prepared using a modified Hummer's method,[35] in which graphite oxide is subjected to chemical exfoliation and ultrasonication. The as-obtained GO sheets are rich in oxygen-rich functional groups, including epoxy, hydroxyl (OH^-) and carboxyl (COO^-) moieties.[38] These oxygen-rich functional groups impart a negative charge to the GO sheets, with the ζ–potential of the aqueous suspension of GO sheets measured to be – 40 mV. The morphology of GO is further characterized by transmission electron microscopy (TEM) and atomic force microscopy (AFM). TEM image of the GO sheets (Fig. S1A) clearly illustrates a flake-like shape with some wrinkled and folded sheet structure at the edge. The GO sheets show a perfect platelet structure with a thickness of about 1 nm (Fig. S1B, C). Separately, Ag nanocubes and octahedra are synthesized via a polyol reduction method, using 1,5-pentanediol as solvent at near-reflux temperature in the presence of poly(vinylpyrrolidone) (PVP) as a stabilizing agent.[34] The as-prepared Ag nanocubes and octahedra are highly monodisperse, with average edge lengths of 121 ± 7 nm and 336 ± 18 nm, respectively (Fig. S2C, D). Citrate-capped spherical Ag nanoparticles with diameters of 150 ± 25 nm are also prepared (Fig. S2B). Thermal evaporated Ag film of ~ 100 nm is used as a control experiment.

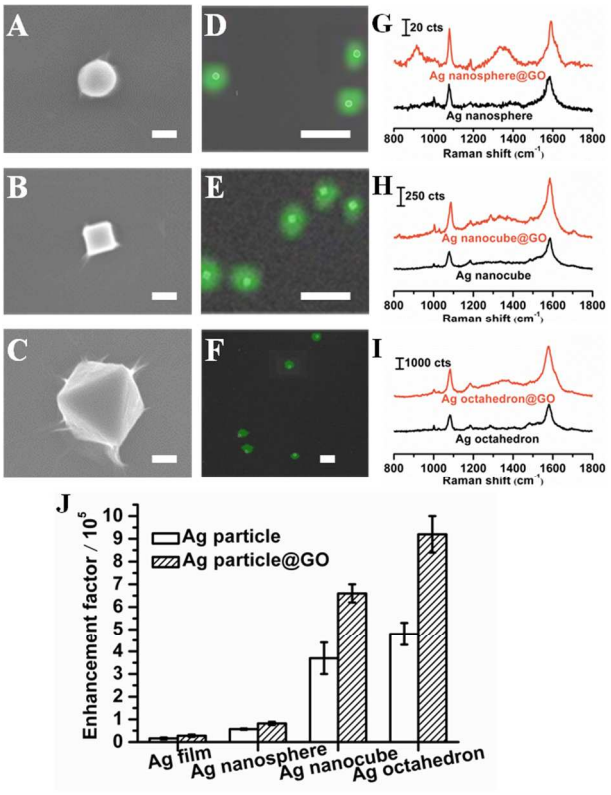

Fig. 2 SEM images of Ag nanoparticle@GO with different Ag nanoparticle morphologies. (A) Ag nanosphere, (B) Ag nanocube, and (C) Ag octahedron. The scale bar is 100 nm for A – C. (D – F) SEM images of isolated Ag particles overlaid with the SERS intensity map, color are assigned by the relative intensity of the spectrum at 1083 cm^{-1}. The scale bar is 1 μm for D – F. (G – I) Corresponding single-particle SERS spectra of 4-MBT adsorbed on Ag nanoparticle (black line) and Ag nanoparticle@GO (orange line). (J) Enhancement factor for 4-MBT of Ag film, Ag nanosphere, Ag nanocube, and Ag octahedron with and without GO coverage.

Hybrid nanostructures of GO and Ag nanoparticles are then fabricated for the subsequent SERS studies (Fig. 1). Ag nanoparticles@GO layout is first used to investigate the effect of nanoparticle morphology on the SERS efficiencies of the hybrid nanoparticles. In this layout, Ag nanoparticles are first ligand

exchanged with 4-methylbenzenethiol (4-MBT) before dispersing them onto an amino-functionalized Si substrate. A dilute GO suspension is then drop-casted onto the nanoparticles to coat a layer of GO around the nanoparticles through electrostatic interactions. The coating of a monolayer of GO around the Ag nanoparticles is characterized using scanning electron microscopy (SEM). SEM images (Fig. 2A – C) of individual Ag nanoparticles obtained at high magnifications clearly show the edges and crumpled silk waves of these carbon sheets, indicating successful immobilization of GO onto the various Ag nanoparticles.

The effect of particle morphology on the SERS capabilities of the hybrid nanostructures is then characterized by comparing the SERS signals of pure Ag nanoparticles and Ag nanoparticles@GO, respectively. 4-methylbenzenethiol (4-MBT) is used as the probe molecule for the SERS experiments because it is known to form a well-defined self-assembled monolayer on the silver surface with a characteristic molecular fingerprint in the Raman spectra.[39] The SERS spectra of 4-MBT collected at an excitation wavelength of 532 nm from various Ag nanoparticles and Ag nanoparticles@GO are shown in Fig. 2G – I. Two Raman peaks can be clearly discerned at 1083 and 1584 cm^{-1} for the pure Ag nanoparticles, with the 1083 cm^{-1} arising from a combination of phenyl ring breathing, C-H in-plane bending and C-S stretching and the 1584 cm^{-1} peak corresponding to phenyl ring stretching of 4-MBT.[40] The 1083 cm^{-1} peak is used for all subsequent analyses because it is free from potential signal interferences that may arise from PVP and/or the G band of GO. Overlays of the Raman maps with the corresponding SEM images (Fig. 2D – F) clearly demonstrate that only single particles are sampled during the SERS measurements. The Raman map corresponds to the SERS intensity of 4-MBT peak at 1083 cm^{-1}. The interparticle spacing is sufficiently large to ensure that there is no plasmon coupling between neighboring particles.

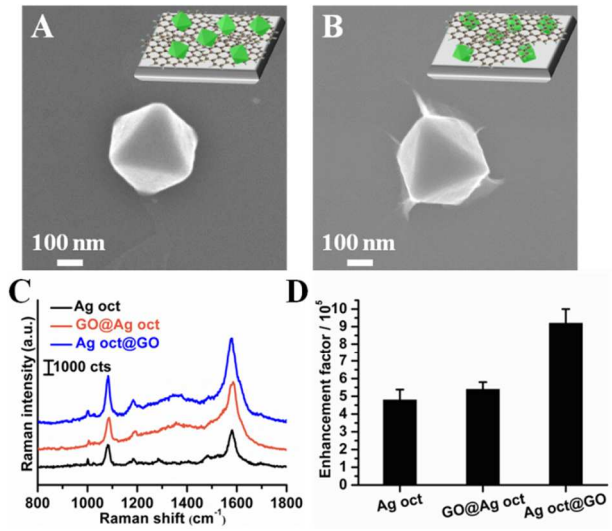

Fig. 3 SEM images of (A) GO@Ag octahedron and (B) Ag octahedron@GO hybrid on Si substrates, and insets show the corresponding schematic illustration of the hybrid layouts. (C) Representative single-particle SERS spectra of 4-MBT on Ag octahedron, GO@Ag octahedron and Ag octahedron@GO, and (D) average single-particle SERS enhancement factor of Ag octahedron, GO@Ag octahedron and Ag octahedron@GO.

Among Ag nanoparticles, both nanocubes and octahedra give rise to stronger SERS signals compared to spherical particles, with Ag octahedra giving rise to the most intense SERS signals (Fig. 2G – H). The single-particle SERS enhancement factors of these particles are estimated to be $(5.7 \pm 0.3) \times 10^4$, $(3.7 \pm 0.7) \times 10^5$, and $(4.8 \pm 0.5) \times 10^5$ for spherical particles, nanocubes and octahedra, respectively for the 1083 cm^{-1} peak (Fig. 2J, see supporting information for detailed calculations). Despite being similar in size, the enhancement factors of nanocubes are 8-fold higher than the spherical particles. This is attributed to the more intense local electromagnetic fields generated around the sharp edges/vertices of the nanocubes.[41] Ag octahedra have the highest enhancement factors due to its much larger dimensions, which make them more effective light scatterers than nanocubes. In comparison, very weak signals are collected from a 100 nm thick thermally evaporated Ag film, which accounts for negligible SERS enhancement (Fig. S3).

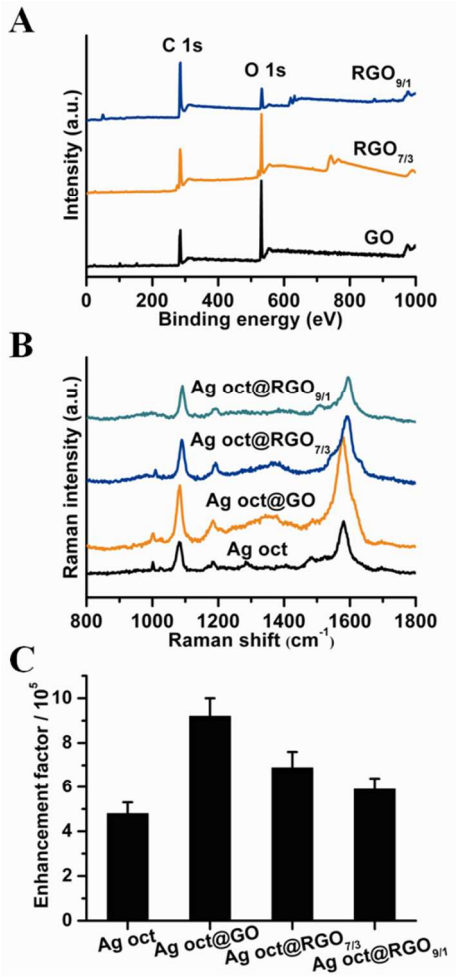

Fig. 4 (A) XPS spectra of GO, $RGO_{7/3}$ and $RGO_{9/1}$. (B) Single-particle SERS spectra of 4-MBT on Ag octahedron, Ag octahedron@GO, Ag octahedron@$RGO_{7/3}$, and Ag octahedron@$RGO_{9/1}$. (C) Average enhancement factor for 4-MBT on Ag octahedron, Ag octahedron@GO, Ag octahedron@ $RGO_{7/3}$, and Ag octahedron@ $RGO_{9/1}$.

When GO is added to the Ag nanoparticles, SERS signals are further enhanced in relation to pure Ag nanoparticles. In addition to the characteristic fingerprints of 4-MBT, a broad scattering peak is also observed at ~1350 cm^{-1} for the Ag

nanoparticles@GO nanostructures. This is indexed to the D band of GO, arising from defects in the curved graphene sheet and staging disorder.[42] On the other hand, the G band overlaps significantly with the phenyl ring stretching of 4-MBT at 1580 cm^{-1}, making it difficult to distinguish the two vibrational modes from each other. A 1 – 2 fold increase in the SERS enhancement factors of Ag nanoparticles@GO is observed in comparison with the pure Ag nanoparticles (Fig. 1J). In the case of both Ag nanocubes@GO and Ag octahedra@GO, the enhancement factor is twice as large as that of the pure Ag nanocubes and octahedra. With the Ag octahedron@GO giving rise to the highest enhancement factor, they are subsequently used as a model system to investigate the SERS characteristics of the hybrid system.

In addition to Ag octahedra@GO layout, we also fabricate GO@Ag octahedra hybrid (Fig. 1) to investigate the influence of GO contact area with Ag octahedra on the enhancement of SERS signals. GO sheets are first adsorbed onto an amino-functionalized Si substrate through electrostatic interactions between negatively-charged GO sheets and positively-charged Si substrate. A dilute suspension of Ag octahedra is then drop-casted onto the GO sheets, giving rise to the GO@Ag octahedra layout. In GO@Ag octahedra, one facet of the Ag octahedra is in direct contact with the GO sheets. This is in contrast with the Ag octahedra@GO structure, where the GO sheets wrap around seven of the eight facets of the Ag octahedra. The successful assembly of Ag octahedra and GO onto the Si substrate is illustrated by SEM images at low (Fig. S4A) and high magnifications (Fig. 3A). GO sheets are hard to distinguish due to their atomic thickness (Fig. 3A). Therefore, AFM measurements are conducted. The AFM image confirms that GO sheets are mostly single layers on the amino-functionalized Si substrate, with average thicknesses of ~ 1 nm measured (Fig. S4C). The areas of Ag octahedra are carefully avoided when measuring AFM images due to the great disparity in the cross-sectional profiles of Ag octahedra and GO. Both hybrid layouts of GO@Ag octahedra and Ag octahedra@GO give rise to enhanced SERS signals as compared to that of pure Ag octahedra (Fig. 3C). The single-particle SERS enhancement factors are determined to be $(5.4 \pm 0.4) \times 10^5$, and $(9.2 \pm 0.8) \times 10^5$ for GO@Ag octahedra and Ag octahedra@GO respectively (Fig. 3D). The SERS signals arising from GO@Ag octahedra is 1.2-fold stronger than pure Ag octahedra, while signals from Ag octahedra@GO are 1.9-fold enhanced using the same comparison.

From the above experiments, it is evident that the presence of GO leads to an additional modest enhancement in the SERS intensities of 4-MBT on Ag octahedra. Furthermore, this enhancement is governed by the extent of GO coverage on the Ag octahedra, with larger GO contact area on Ag octahedra, as observed in the case of Ag octahedra@GO, leading to higher enhancement. Chemical enhancement is a short-range effect occurring on the molecular scale, requiring the molecule to be in contact with or in close proximity to the substrate to enable charge transfer between the molecule and the substrate.[15] Put together, these observations suggest that the nature of this additional enhancement stems from a chemical effect. Chemical enhancement from GO has been shown to arise from π - π stacking and charge transfer from the lone-pairs of electrons on the oxygen-containing moieties to the probe molecules.[21]

Table 1. List of Raman shift, SERS intensity, enhancement factor and enhancement factor ratio of 4-ATP, 4-MBT and 4-MBA on pure Ag octahedron and Ag octahedron@GO.

	4-ATP		4-MBT		4-MBA	
	Ag oct	Ag oct@GO	Ag oct	Ag oct@GO	Ag oct	Ag oct@GO
Raman shift (cm^{-1})	1083	1077	1077	1083	1087	1089
Raman intensity	1044±157	2502±168	1233±135	2359±220	1358±113	2198±198
Enhancement factor	$(4.1\pm0.6)\times10^4$	$(9.8\pm0.6)\times10^5$	$(4.8\pm0.5)\times10^5$	$(9.2\pm0.8)\times10^5$	$(5.3\pm0.4)\times10^4$	$(8.6\pm0.8)\times10^5$
Enhancement factor ratio	2.4		1.9		1.6	

To probe the mechanism of SERS enhancement brought about by the addition of GO, we tune the surface charges of GO by subjecting GO to various degrees of reduction. Reducing GO decreases the number of oxygen-rich functional groups present on GO. If the additional SERS enhancement from Ag octahedra@GO is due to a charge transfer process from the oxygen-rich functional groups, then the decrease in oxygen-rich functional groups will give rise to a corresponding decrease in SERS signals. GO is reduced to $RGO_{7/3}$ and $RGO_{9/1}$ with different reduction extents by varying the reducing time. The subscripts following the RGO labels describes the atomic C/O ratio of the reduced GO. The extent of GO reduction is characterized by XPS (Fig. 4A). The atomic C/O ratio increases with increasing reduction extent, indicating a decrease in the oxygen-rich functional groups on GO. The calculated oxygen atomic content is about 40 %, 30 % and 10 % for GO, $RGO_{7/3}$ and $RGO_{9/1}$, respectively. Additionally, from the C 1s spectra of GO, $RGO_{7/3}$ and $RGO_{9/1}$ (Fig. S5), five different peaks centered at 284.5, 285.6, 286.7, 287.8, and 288.8 eV are observed, corresponding to sp^2 C, sp^3 C, C-O, -C=O, and COO^- groups, respectively.[43] Compared with GO, the intensities of all C 1s peaks of the carbons binding to oxygen and the peak of sp^3 carbon of $RGO_{7/3}$ and $RGO_{9/1}$ decrease remarkably, revealing that most of the oxygen-containing functional groups are removed and the conjugated graphene networks are restored.[44]

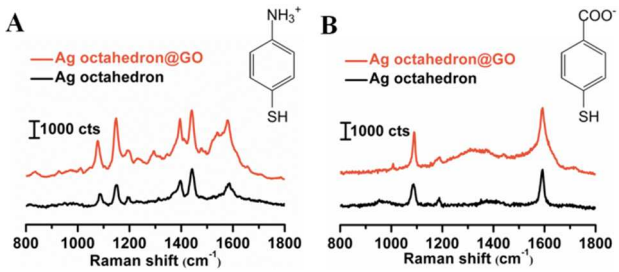

Fig. 5 Single-particle SERS spectra of (A) 4-ATP- and (B) 4-MBA-functionalized on Ag octahedron and Ag octahedron@GO.

SERS intensities measured for the hybrid nanostructures of Ag octahedra@RGO with increasing degrees of reduction show that the intensities of the 4-MBT peaks become monotonically weaker (Fig. 4B). For the Ag octahedra@$RGO_{9/1}$ with 10 atomic% oxygen on RGO sheets, the enhancement factor for 4-MBT decreased about 35% to $(5.9 \pm 0.5) \times 10^5$ as compared to that of Ag octahedra@GO. Correlating the decrease in SERS signals with the decrease in number of oxygen-rich species on RGO, it can be concluded that the charge transfer process between the oxygen-functional groups and probe molecules is the dominant mechanism contributing to the additional SERS enhancement observed from the hybrid nanostructures when compared to pure Ag nanoparticles.

Table 2. SERS enhancement factor ratio between Ag octahedron@GO and Ag octahedron and the assignments of several Raman bands of the Raman probe molecules.

Probe molecules	Raman shift	Enhancement factor ratio	Band asignment
R6G	1195	4.4	C-H bending
	1362	4.0	xanthene ring stretching
	1509	3.6	xanthene ring stretching
	1575	3.1	xanthene ring stretching
	1649	3.8	xanthene ring stretching
CV	1178	2.8	ring C-H bending
	1374	3.1	N-phenyl stretching
	1588	2.5	ring C–C stretching
	1620	2.7	ring C-C stretching

In addition to using RGO to probe the effect of chemical enhancement in the hybrid Ag octahedra@GO nanostructures, the probe molecules are also varied. 4-aminothiophenol (4-ATP) and 4-mercaptobenzoic acid (4-MBA), carrying a positive and negative charge respectively, are used in place of the neutral 4-MBT. Fig. 5 shows the SERS spectra from both pure Ag octahedra as well as from Ag octahedra@GO nanostructures. The corresponding data on SERS enhancement is summarized in Table 1. The Raman shift of 4-ATP is at 1083 cm^{-1} on Ag octahedra, while it shifts to 1077 cm^{-1} after the coverage of GO. This downshift likely arises from the charge transfer between GO and 4-ATP, where the electrons transfer from 4-ATP to GO.[17] The change in the Raman shift and SERS enhancement of 4-ATP on Ag octahedron@GO is more obvious than 4-MBA and 4-MBT. The enhancement effect of GO coverage was quantitative analyzed by applying enhancement factor ratio between the two substrates. The extent of signal enhancement varies for the differently charged molecules, with the positively charged 4-ATP demonstrating the highest signal enhancement of 2.4-fold. In contrast, lower enhancement ratio is measured from 4-MBT (1.9-fold) and 4-MBA (1.6-fold), which is either neutral or carries identical charge with GO. The 2.4-fold enhancement from 4-ATP is due to favorable electrostatic interactions between the oppositely charged 4-ATP and GO sheets. In our system, the effect of chemical enhancement from metallic nanoparticles is taken to be comparable among these two molecules because of the similar SERS enhancement factors observed from these two molecules on pure Ag octahedra. Therefore, this phenomenon can be rationalized by the different affinity of the two molecules with GO sheets. The positively charged 4-ATP molecule has strong electrostatic attraction with the negatively charged GO sheets, which facilitates the charge transfer process. In contrast, negatively charged 4-MBA molecules interacts weakly with GO. As a consequence, SERS enhancement induced by charge transfer between GO and probe is more favorable for the positively charged 4-ATP.

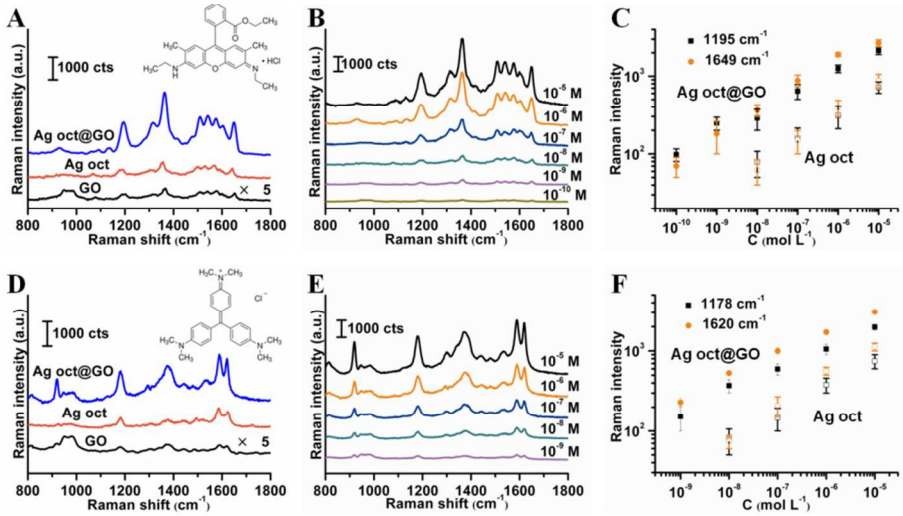

Fig. 6 SERS signals of 1×10^{-6} M (A) R6G, and (D) CV on different SERS substrates: GO (black line), Ag octahedron (orange line) and Ag octahedron@GO (blue line), respectively. The insets show the structures of R6G and CV, respectively. SERS spectra of R6G (B) and CV (E) deposited on Ag octahedron@GO by soaking in the solution with different concentrations labeled in the respective SERS spectra. (C, F) The corresponding plots of Raman intensity versus concentration. Solid points are for Ag octahedron@GO and hollow points for Ag octahedron.

Thus far, we have demonstrated that by combining GO with Ag octahedra, the overall SERS signals of the hybrid nanostructures are enhanced compared to pure Ag octahedra due to an additional component of chemical enhancement originating from the interactions of GO with the probe molecules. In the final part of this study, we examine single-particle SERS sensing

performance of the Ag octahedra@GO nanostructures. For this, we have chosen two aromatic molecules, rhodamine 6G (R6G) and crystal violet (CV), as the probe molecules. These two molecules also possess well-defined molecular fingerprints in their Raman spectra and are commonly employed as probes for evaluating the sensing capabilities of various systems.[45,46] These organic molecules are deposited onto Ag octahedra@GO nanostructures by immersing the sample in dye solutions of various concentrations for 2 h. The substrate is then rinsed to remove the unbound dye molecules and dried using a nitrogen stream.

SERS spectra of both R6G and CV at 1 μM measured from pure Ag octahedra, pure GO and Ag octahedra@GO are shown in Fig. 6A, D. The characteristic vibrational modes of both molecules are indexed in Table 2. For the C-H bending modes, SERS signals from Ag octahedra@GO are approximately 30-fold enhanced compared to pure GO and nearly 3 – 4-fold enhanced relative to pure Ag octahedra for both molecules. The superior sensing capability of the Ag octahedra@GO is once again demonstrated with these aromatic molecules. The effect of chemical enhancement is slightly higher than the thiol probe molecules due to the more effective $\pi - \pi$ interactions between the dye molecules and GO.[24] The detection limits and linearity range of the single particle Ag octahedra@GO SERS sensing are also studied. The detection limits for R6G is monitored using the 1195 cm^{-1} and 1649 cm^{-1} bands and SERS signals (with signal/noise ratio >3) can still be detected from the single-particle measurements down to 0.1 nM, which is two orders of magnitude lower than that of pure Ag octahedra (Fig. 6B, C). This low detection limit may be due to the increased adsorption force, both physically and chemically between aromatic molecules and GO sheets, especially at low concentrations.[16] Both the enrichment effect of molecules and their chemical interactions with GO sheets should be taken into consideration.[47] The linearity range spans across 6 orders of magnitude, from 0.1 nM to 10 μM. The detection limits for CV (Fig. 6E, F) are also decreased to 1 nM, which is one order of magnitude lower as compared to that of pure Ag octahedra using the vibrational modes at 1178 cm^{-1} and 1620 cm^{-1}. The detection limits obtained using both dye molecules in our experiment is comparable to the ones reported in the literature.[48,49] However, it should be noted that the measurements in our study are conducted on single Ag octahedra rather than single GO sheets decorated with numerous small metallic nanoparticles with large-area SERS hotspots. As such, the detection limits can certainly be lowered further by using octahedra dimers or nanoparticle clusters decorated with GO sheets.

4. Conclusions

In summary, hybrid nanostructures integrating GO and various shape-controlled Ag nanoparticles have been fabricated successfully. Such GO and shape-controlled Ag nanoparticles hybrid nanostructures are excellent candidates for single-particle SERS substrate. The role of particle morphology on the SERS capabilities of Ag nanoparticle@GO hybrid nanostructures is investigated and it is found that strongest signals are measured from hybrid nanostructures fabricated with Ag octahedra. This is due to the presence of multiple sharp tips/edges as well as the large dimensions of the octahedra, making Ag octahedra efficient light scatterers. In all cases, SERS signals of the Ag octahedra@GO nanostructures are enhanced by 1-2 folds when compared with pure Ag octahedra. The mechanism of this additional signal enhancement is determined to be chemical in nature. This is verified from additional experiments conducted by changing the surface coverage of GO on Ag octahedra, by using reduced GO in place of GO as well as by changing the probe molecules used. Finally, we demonstrate the potential of single-particle SERS sensing of aromatic molecules with our hybrid nanostructures and find that detection limits down to nM-levels can be achieved for both R6G and CV. Therefore, our work investigating SERS capabilities at the single particle level is crucial for direct probing of the chemical effect of GO on plasmonic nanoparticles, thus gives fundamental study for the enhancement mechanism of GO in SERS applications. Moreover, the as-prepared GO and shape-controlled Ag nanoparticles hybrids provides new opportunities for chemical and biological sensing applications. Our study is expected to shed light on the fundamental mechanism of the SERS effect as well as efficiently improve SERS performance towards applications.

Acknowledgements

X.Y.L. thanks the supports from National Research Foundation, Singapore (NRF-NRFF2012-04), Nanyang Technological University's start-up grant. T.L. and F.W. are grateful for the financial support from the National Natural Science Foundation of China (51125011).

Notes and references

[a]*Division of Chemistry and Biological Chemistry, School of Physical and Mathematical Sciences, Nanyang Technological University, 21 Nanyang Link, Singapore 637371, Singapore. E-mail: xyling@ntu.edu.sg; Tel: +65-6513 2740*

[b]*State Key Laboratory of Molecular Engineering of Polymers, Department of Macromolecular Science, Fudan University, 220 Handan Road, Shanghai 200433, P. R. China. Email: txliu@fudan.edu.cn; Tel: +86-21-55664197*

† Electronic supplementary information (ESI) available: Detailed calculation of enhancement factor, TEM and AFM images of GO, SEM images of Ag film fabricated by vacuum thermal evaporation, Ag nanospheres, Ag nanocubes and Ag octahedra, the corresponding SERS spectra of 4-MBT adsorbed on Ag film and Ag film@GO. SEM images of GO@Ag octahedra and Ag octahedra@GO hybrid on Si substrates, AFM image and corresponding height profile of GO@Ag octahedra, curve fit of C1s spectra of GO, $RGO_{7/3}$, and $RGO_{9/1}$, SERS spectra of 10^{-10} M R6G and 10^{-9} M CV deposited on Ag octahedron@GO, SERS spectra of R6G and CV on deposited Ag octahedron by soaking in the solution with different concentrations. See DOI: 10.1039/b000000x/

1 S. M. Nie and S. R. Emery, *Science*, 1997, **275**, 1102-1106.
2 M. E. Stewart, C. R. Anderton, L. B. Thompson, J. Maria, S. K. Gray, J. A. Rogers and R. G. Nuzzo, *Chem. Rev.*, 2008, **108**, 494-521.
3 B. Sharma, R. R. Frontiera, A. I. Henry, E. Ringe and R. P. Van Duyne, *Mater. Today*, 2012, **15**, 16-25.
4 H. Ko, S. Singamaneni and V. V. Tsukruk, *Small*, 2008, **4**, 1576-1599.
5 D. Y. Wu, X. M. Liu, S. Duan, X. Xu, B. Ren, S. H. Lin and Z. Q. Tian, *J. Phys. Chem. C*, 2008, **112**, 4195-4204.
6 S. Lecomte, P. Matejka and M. H. Baron, *Langmuir*, 1998, **14**, 4373-4377.
7 W. E. Doering and S. M. Nie, *J. Phys. Chem. B*, 2002, **106**, 311-317.

8 K. A. Willets and R. P. Van Duyne, *Annu. Rev. Phys. Chem.*, 2007, **58**, 267-297.

9 J. Zhao, A. O. Pinchuk, J. M. Mcmahon, S. Z. Li, L. K. Ausman, A. L. Atkinson and G. C. Schatz, *Acc. Chem. Res.*, 2008, **41**, 1710-1720.

10 M. Rycenga, C. M. Cobley, J. Zeng, W. Y. Li, C. H. Moran, Q. Zhang, D. Qin and Y. N. Xia, *Chem. Rev.*, 2011, **111**, 3669-3712.

11 L. Rodriguez-Lorenzo, R. A. Alvarez-Puebla, I. Pastoriza-Santos, S. Mazzucco, O. Stephan, M. Kociak, L. M. Liz-Marzan and F. J. G. Abajo, *J. Am. Chem. Soc.*, 2009, **131**, 4616–4618.

12 Y. Yang, S. Matsubara, L. M. Xiong, T. Hayakawa and M. Nogami, *J. Phys. Chem. C*, 2007, **111**, 9095-9104.

13 M. Rycenga, P. Camargo, W. Y. Li, C. H. Moran and Y. N. Xia, *J. Phys. Chem. Lett.*, 2010, **1**, 696-703.

14 K. L. Kelly, E. Coronado, L. L. Zhao and G. C. Schatz, *J. Phys. Chem. B*, 2003, **107**, 668-677.

15 X. Ling, L. M. Xie, Y. Fang, H. Xu, H. L. Zhang, J. Kong, M. S. Dresselhaus, J. Zhang and Z. F. Liu, *Nano Lett.*, 2010, **10**, 553-561.

16 W. G. Xu, N. N. Mao and J. Zhang, *Small*, 2013, **9**, 1206-1224.

17 X. Ling and J. Zhang, *Small*, 2010, **6**, 2020-2025.

18 X. Ling, L. G. Moura, M. A. Pimenta and J. Zhang, *J. Phys. Chem. C*, 2012, **116**, 25112-25118.

19 X. Ling, J. X. Wu, L. M. Xie and J. Zhang, *J. Phys. Chem. C*, 2013, **117**, 2369-2376.

20 S. Huh, J. Park, Y. S. Kim, K. S. Kim, B. H. Hong and J. M. Nam, *ACS Nano*, 2011, **5**, 9799-9806.

21 X. X. Yu, H. B. Cai, W. H. Zhang, X. J. Li, N. Pan, Y. Luo, X. P. Wang and J. G. Hou, *ACS Nano*, 2011, **5**, 952-958.

22 W. G. Xu, X. Ling, J. Q. Xiao, M. S. Dresselhaus, J. Kong, H. X. Xu, Z. F. Liu and J. Zhang, *Proc. Natl. Acad. Sci. USA*, 2012, **109**, 9281-9286.

23 W. G. Xu, J. Q. Xiao, Y. F. Chen, Y. B. Chen, X. Ling and J. Zhang, *Adv. Mater.*, 2013, **25**, 928-933.

24 X. J. Liu, L. Y. Cao, W. Song, K. L. Ai and L. H. Lu, *ACS Appl. Mater. Interfaces*, 2011, **3**, 2944-2952.

25 Y. K. Kim, S. W. Han and D. H. Min, *ACS Appl. Mater. Interfaces*, 2012, **4**, 6545-6551.

26 X. K. Kong, Q. W. Chen and Z. Y. Sun, *Chem. Phys. Lett.*, 2013, **564**, 54-59.

27 Z. Zhang, F.G. Xu, W. S. Yang, M. Y. Guo, X. D. Wang, B. L. Zhang and J. L. Tang, *Chem. Commun.*, 2011, **47**, 6440-6442.

28 G. Lu, H. Li, C. Liusman, Z. Y. Yin, S. X. Wu and H. Zhang, *Chem. Sci.*, 2011, **2**, 1817-1821.

29 Y. W. Zhang, S. Liu, L. Wang, X. Y. Qin, J. Q. Tian, W. B. Lu, G. H. Chang and X. P. Sun, *RSC Adv.*, 2012, **2**, 538-545.

30 B. Zhao, Z. R. Liu, W. Y. Fu and H. B. Yang, *Electrochem. Commun.*, 2013, **27**, 1-4.

31 W. Ren, Y. X. Fang and E. K. Wang, *ACS Nano*, 2011, **5**, 6425-6433.

32 X. F. Ding, L. T. Kong, J. Wang, F. Fang, D. D. Li and J. H. Liu, *ACS Appl. Mater. Interfaces*, 2013, **5**, 7072-7078.

33 Y. M. Wu, W. J. Xu, Y. Wang, Y. L. Yuan and R. Yuan, *Electrochim. Acta*, 2013, **88**, 135-140.

34 T. H. Kim, K. B. Lee and J. W. Choi, *Biomaterials*, 2013, **34**, 8660-8670.

35 N. I. Kovtyukhova, P. J. Ollivier, B. R. Martin, T. E. Mallouk, S. A. Chizhik, E. V. Buzaneva and A. D. Gorchinskiy, *Chem. Mater.*, 1999, **11**, 771-778.

36 A. Tao, P. Sinsermsuksakul and P. D. Yang, *Angew. Chem. Int. Ed.*, 2006, **45**, 4597-4601.

37 P. C. Lee and D. Meisel, *J. Phys. Chem.*, 1982, **86**, 3391-3395.

38 D. R. Dreyer, S. Park, C. W. Bielawski and R. S. Ruoff, *Chem. Soc. Rev.*, 2010, **39**, 228-240.

39 M. S. Chen, I. Y. Phang, M. R. Lee, J. Yang and X. Y. Ling, *Langmuir*, 2013, **29**, 7061-7069.

40 M. Rycenga, M. H. Kim, P. Camargo, C. Cobley, Z. Y. Li and Y. N. Xia, *J. Phys. Chem. A*, 2009, **113**, 3932-3939.

41 J. M. McLellan, A. Siekkinen, J. Y. Chen and Y. N. Xia, *Chem. Phys. Lett.*, 2006, **427**, 122-126.

42 C. Z. Zhu, S. J. Guo, Y. X. Fang and S. J. Dong, *ACS Nano*, 2010, **4**, 2429-2437.

43 Z. J. Fan, W. Kai, J. Yan, T. Wei, L. J. Zhi, J. Feng, Y. M. Ren, L. P. Song and F. Wei, *ACS Nano*, 2011, **5**, 191-198.

44 C. Z. Zhu, S. J. Guo, Y. X. Fang and S. J. Dong, *ACS Nano*, 2010, **4**, 2429-2437.

45 M. Mulvihill, A. Tao, K. Benjauthrit, J. Arnold and P. Yang, *Angew. Chem. Int. Ed.*, 2008, **47**, 6456-6460.

46 A. Kim, S. J. Barcelo, R. S. Williams and Z. Y. Li, *Anal. Chem.*, 2012, **84**, 9303-9309.

47 X. K. Kong and Q. W. Chen, *J Mater. Chem.*, 2012, **22**, 15336-15341.

48 E. Galopin, J. Barbillat, Y. Coffinier, S. Szunerits, G. Patriarche and R. Boukherroub, *ACS Appl. Mater. Interfaces*, 2009, **1**, 1396-1403.

49 Y. C. Liu, C. C. Yu and S. F. Sheu, *J. Mater. Chem.*, 2006, **16**, 3546-3551.